Anisotropic hinge model for polarization-mode dispersion in installed fibers

Jinglai Li,[1] Gino Biondini,[2,*] William L. Kath,[1] and Herwig Kogelnik[3]

[1]*Department of Engineering Sciences and Applied Mathematics, Northwestern University, Evanston, Illinois 60208, USA*

[2]*Department of Mathematics, State University of New York at Buffalo, Buffalo, New York 14260, USA*

[3]*Bell Laboratories, Alcatel-Lucent, Holmdel, New Jersey 07733, USA*

**Corresponding author: biondini@buffalo.edu*

Received June 2, 2008; revised July 7, 2008;
posted July 23, 2008 (Doc. ID 96867); published August 14, 2008

We discuss a generalized waveplate hinge model to characterize anisotropic effects associated with the hinge model of polarization-mode dispersion in installed systems. In this model, the action of the hinges is a random time-dependent rotation about a fixed axis. We obtain the probability density function of the differential group delay and the outage probability of an individual wavelength band using a combination of importance sampling and the cross-entropy method, and we then compute the noncompliant capacity ratio by averaging over wavelength bands. The results show that there are significant differences between the outage statistics predicted by isotropic and anisotropic hinge models. © 2008 Optical Society of America

OCIS codes: 060.2330, 060.4510.

Recent experimental investigations of polarization-mode dispersion (PMD) in wavelength-division-multiplexed (WDM) installed systems have found variations in the temporal statistics of the differential group delay (DGD) of different wavelength bands [1]. This behavior is consistent with the so-called "hinge model" of PMD [1–4] in which systems are composed of a concatenation of a relatively small number of long stable fiber sections joined by short unprotected sections, or "hinges," which are subject to environmental effects. The DGD of each stable section is assumed to follow a Maxwellian distribution with respect to wavelength and to be frozen in time. The hinges themselves bring little or no contribution to the total DGD, but they scatter the PMD vector across the Poincaré sphere, and their fluctuations are responsible for the temporal dynamics of PMD within each channel. The measured statistics of PMD-induced transmission outages of systems described by the hinge model differ from those of traditional models in that they contradict the assumption that all channels have an identical outage probability.

A common assumption in the hinge model is that the hinges act as polarization controllers that scatter the PMD vector uniformly across the Poincaré sphere. We will refer to this as the isotropic hinge model. System outages for the hinge model have been well studied under the isotropic assumption. Recent experimental observations [5], however, suggest that the hinges do not scatter the PMD vector across all of the Poincaré sphere but rather act more like rotators, that is, like elements that rotate the PMD vector about a fixed axis. This action is consistent with theoretical studies of the behavior of arbitrary polarization elements [6], which show that, to first order with respect to variations of any parameter, any polarization element behaves like a rotator. Based on these experimental results and theoretical observations, here we therefore study an anisotropic hinge model in which the stable sections are joined by "waveplate-type" hinges that produce a random time-dependent rotation about a static rotation axis. As we show below, the statistics of PMD in this model differ significantly from those in the isotropic model.

At each wavelength, the total PMD for a finite number of sections is determined by the PMD concatenation equations. For first-order PMD, this is [7]

$$\vec{\tau}_{n+1} = \mathsf{R}_{n+1}\mathsf{H}_n\vec{\tau}_n + \Delta\vec{\tau}_{n+1}. \tag{1}$$

Here $\vec{\tau}_n$ is the total PMD vector after the nth section, the fixed vector $\Delta\vec{\tau}_n$ is the PMD vector of the nth section, R_{n+1} is the rotation matrix of the $(n+1)$st section, and H_n is the rotation matrix of the nth hinge. The PMD vector $\Delta\vec{\tau}_n$ of each section is uniformly distributed on the Poincaré sphere but is frozen in time, and the DGD $\Delta\tau_n = |\Delta\vec{\tau}_n|$ of each section obeys a Maxwellian distribution with respect to wavelength. If one is interested only in the length of the total PMD vector, it is possible to eliminate R_{n+1} from Eq. (1) by defining $\vec{\tau}'_{n+1} = \mathsf{R}_{n+1}^{-1}\vec{\tau}_{n+1}$, $\Delta\vec{\tau}'_{n+1} = \mathsf{R}_{n+1}^{-1}\Delta\vec{\tau}_{n+1}$, and $\mathsf{H}'_n = \mathsf{H}_n\mathsf{R}_n$. As a result,

$$\vec{\tau}'_{n+1} = \mathsf{H}'_n\vec{\tau}'_n + \Delta\vec{\tau}'_{n+1}, \tag{2}$$

where the $\Delta\vec{\tau}'_n$ are also uniformly distributed on the Poincaré sphere. In what follows, we will omit the primes for simplicity. The only temporal variation in Eq. (2) arises from the hinge rotation matrix H_n. In the isotropic hinge model it is assumed that the hinges scatter the previous PMD vector $\vec{\tau}_n$ randomly and uniformly across the Poincaré sphere. Based on [5,6], however, here we assume that the nth hinge describes a rotation about a fixed axis $\hat{r}_n = (r_n^1, r_n^2, r_n^3)$ that is arbitrarily distributed on the Poincaré sphere with respect to wavelength with a rotation angle φ_n that is randomly and dynamically varying. Thus, the rotation matrix H_n becomes [7]

$$\mathsf{H}_n = \cos\varphi_n\mathsf{I} + (1-\cos\varphi_n)\hat{r}_n\hat{r}_n^t + \sin\varphi_n\hat{r}_n\times, \tag{3}$$

where I is the 3×3 identity matrix, $\hat{r}\hat{r}^t$ is the dyadic matrix, and $\vec{r}\times$ is the cross-product matrix [7].

By analogy with the behavior of a wave plate, we refer to this as the waveplate hinge model. Note however that, unlike ordinary wave plates, the rotation axes $\hat{r}_n$ are not confined to the equator of the Poincaré sphere. (This statement applies even when the hinges are actual wave plates because of the arbitrary rotation introduced when going from H_n to H'_n.) Thus, one should think of the hinges as generalized waveplates. We reiterate that Eq. (3) describes the response of any polarization element to first-order with respect to variations of any of its parameters [6].

It is difficult to use either standard Monte Carlo (MC) simulations or laboratory measurements to fully assess system outage probabilities owing to the extremely large number of PMD configurations that must be visited to obtain reliable estimates. Importance sampling (IS) has been used to address this problem and allow efficient computation of PMD-induced transmission penalties [8–10]. The idea is to implement MC simulations using a biased distribution $p^*(\mathbf{x})$ of the random variable $\mathbf{x}$ instead of the true distribution $p(\mathbf{x})$ so that large DGDs occur more frequently than they would normally while correcting for the bias using the likelihood ratios. In our case the vector $\mathbf{x}$ collects the rotation angles $\varphi_1, \ldots, \varphi_{N-1}$ of all the hinge rotation matrices H_n.

The fundamental issue in IS is of course to design a good biasing strategy. In contrast to previous studies [8–10], to the best of our knowledge it is not possible to identify the optimal biasing directions analytically for the waveplate hinge model, because the PMD dynamics are more complicated. To overcome this difficulty we use the cross-entropy (CE) method. It is well known that an optimal biasing distribution exists in principle; $p^*_{\text{opt}}(\mathbf{x}) = I(\mathbf{x})p(\mathbf{x})/P$, where the indicator function $I(\mathbf{x})$ equals 1 if $\mathbf{x}$ is in the region of interest and 0 otherwise and where P is the sought-after probability. This result is not useful by itself as it requires knowledge of the unknown quantity P. One can, however, find a good biasing distribution by requiring that it be "close" to the optimal biasing distribution in terms of some measure of distance. The CE (or Kullback–Leibler distance) between two distributions [11] is a good choice for such a measure:

$$\mathcal{D}(p^*_{\text{opt}}, p^*) = \mathbb{E}_{p^*_{\text{opt}}}[\ln(p^*_{\text{opt}}(\mathbf{x})/p^*(\mathbf{x}))], \tag{4}$$

where $\mathbb{E}_p$ is the expectation value with respect to a density p. Although $\mathcal{D}(p^*_{\text{opt}}, p^*)$ itself cannot be evaluated directly (because p^*_{opt} depends on P), the direction of its gradient is independent of P and can therefore be evaluated even without its knowledge. In this way, one can determine a good biasing distribution $p^*(\mathbf{x})$ by minimizing the distance between it and the optimal distribution $p^*_{\text{opt}}(\mathbf{x})$ [11]. In summary, the method to be used for the simulations consists of: (i) first searching for a good biasing distribution $p^*(\mathbf{x})$ by minimizing the CE distance between it and $p^*_{\text{opt}}(\mathbf{x})$ and (ii) then applying IS using the distribution $p^*(\mathbf{x})$. The implementation and simulation details are beyond the scope of this Letter and will be discussed elsewhere.

We used IS-CE simulations to reconstruct the probability density function (PDF) of the total DGD in the waveplate hinge model. We considered transmission links consisting of ten sections, a mean DGD of 3 ps, and sectional PMD vectors and rotation axes uniformly distributed across the Poincaré sphere but frozen while the hinge rotation angles were randomly varying and uniformly distributed in $[0, 2\pi]$. Figure 1 compares the PDF of the DGD for the isotropic model [12] with that for the waveplate hinge model (with two different sets of hinge rotation axes) with the same sectional PMD vectors. Note that for each choice of sectional PMD vectors there are infinitely many PDFs for the waveplate hinge model (one for each specific realization of hinge rotation axes). The IS-CE simulations agree with unbiased MC simulations (not shown) of the waveplate model where the latter give results. Also, as in the isotropic model, one observes convergence to the Maxwellian distribution as the number of sections tends to infinity in simulations of the waveplate hinge model.

To estimate the outage probability we used the outage map method [13]. Namely, for each wavelength band, we expressed the first-order PMD-induced outage probability as

$$P_{\text{out}} = \int_0^\infty \int_{\gamma_1(\tau)}^{\gamma_2(\tau)} p(\tau, \gamma) \mathrm{d}\gamma \mathrm{d}\tau, \tag{5}$$

where τ is the total DGD and γ is the power splitting ratio, $p(\tau, \gamma)$ is their joint PDF, and $[\gamma_1(\tau), \gamma_2(\tau)]$ is the range of values of the power splitting ratios that result in an outage (namely, the values for which the PMD-induced penalty exceeds a prescribed value ε) as obtained from detailed numerical simulations [13]. Assuming a uniform distribution of γ (which implies the presence of an isotropic polarization scatterer at the input of the system), the inner integral in Eq. (5) simply yields $p_{\text{dgd}}(\tau)\Delta\gamma(\tau)$, where $p_{\text{dgd}}(\tau)$ is the PDF of

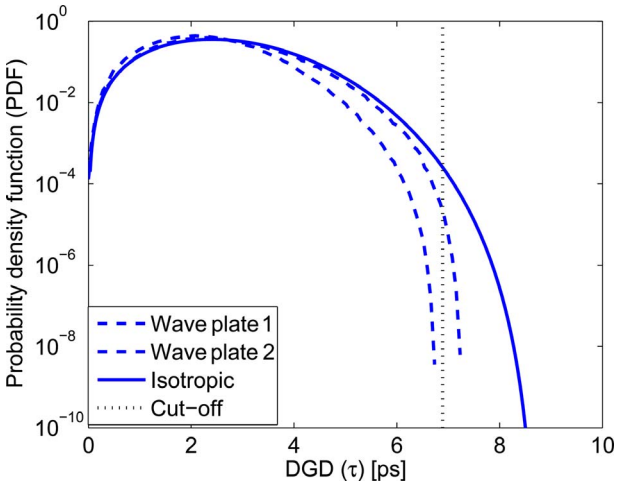

Fig. 1. (Color online) Comparison of the PDF of the DGD for the waveplate hinge model (dashed curve, for two sets of hinge directions) versus that for the isotropic hinge model (solid curve). Each case uses the same set of ten sectional PMD vectors. The vertical line indicates the cut-off value $\tau_o = 6.89$ ps, which is the outage threshold for a system with a 1 dB penalty margin.

the DGD and $\Delta\gamma = \gamma_2(\tau) - \gamma_1(\tau)$. A good approximation for $\Delta\gamma$ has been found to be [13]

$$\Delta\gamma(\tau) = \sqrt{1 + \frac{4\alpha\varepsilon}{A}}\sqrt{1 - \left(\frac{\tau_0}{\tau}\right)^2} \tag{6}$$

for $\tau_o < \tau < \tau_1$, with $\Delta\gamma(\tau) = 0$ for $\tau < \tau_o$ and $\Delta\gamma(\tau) = 1$ for $\tau > \tau_1$, where $\tau_o = 2T/\sqrt{A/\varepsilon + 4\alpha}$ and $\tau_1 = T/\sqrt{\alpha}$. Here T is the bit period, and A and α depend on the modulation format. Note that Eq. (6) implies that outages can only take place when $\tau > \tau_o$. An upper bound for the outage probability, which removes the requirement for an input scatterer, can also be obtained by taking $\Delta(\gamma) = 1$ for all $\tau > \tau_o$.

We considered a link of ten sections with a mean DGD of 3 ps (as before) using the non-return-to-zero format at 40 Gb/s, corresponding to $A = 51$, $\alpha = 0.41$, and $T = 25$ ps and an allocated power margin ε of 1 dB. With these parameters, the cut-off value is $\tau_o = 6.89$ ps. So a channel represented by one of the dashed curves on the left in Fig. 1 is outage-free in the waveplate hinge model, although it is not in the isotropic hinge model (solid curve). The results also show that, for the same set of section lengths, the waveplate hinge model predicts a larger fraction of outage-free channels than the isotropic hinge model.

The noncompliant capacity ratio (NCR) was introduced in [13] to characterize the outage statistics of a WDM system, where PMD follows the hinge model. Specifically, the NCR is defined as the fraction of wavelength bands that are noncompliant with a given outage specification. In Fig. 2 we compare the NCR predicted by the isotropic hinge model with that predicted by the waveplate hinge model from an MC simulation of 10,000 wavelength bands (with a different set of sectional PMD vectors and hinge rotation axes for each band). The NCR in the limit of an infinite number of sections is also shown and is a step function, namely, NCR = 1 for $P_{\text{spec}} < P_{\text{out}}$ and NCR = 0 otherwise. Some differences are visible between the upper bound and the values obtained assuming uniform splitting ratios. Nonetheless, at the small outage probabilities that are of practical interest (to the right in Fig. 2) the values of NCR for the waveplate hinge model are significantly smaller than those from the isotropic model. Therefore, in this regime the isotropic hinge model overestimates the NCR compared with the waveplate hinge model. Similar results also arise for transmission links with different numbers of sections.

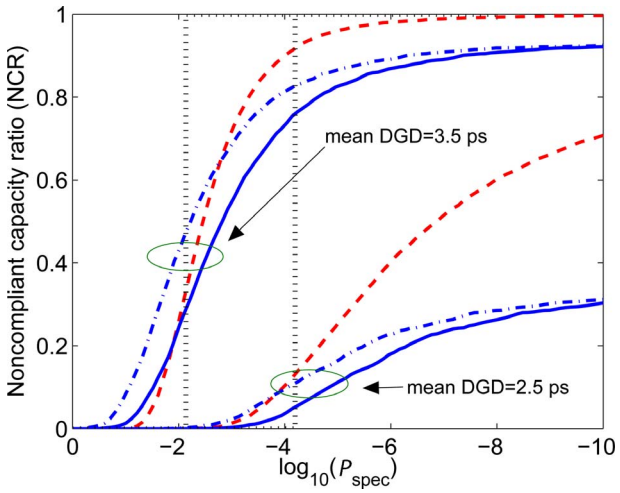

Fig. 2. (Color online) NCR as a function of the specified outage probability for transmission links with ten sections and a mean DGD 3.5 (top left curves) and 2.5 ps (bottom right curves). Dashed lines, NCR in the isotropic model; solid lines, NCR in the anisotropic model assuming uniform splitting ratios; dotted–dashed curves, upper bound for the NCR in the anisotropic model; vertical lines, transition between NCR = 0 and NCR = 1 in the traditional model of PMD.

In summary, we have proposed a waveplate hinge model to characterize anisotropic effects associated with polarization hinges in installed optical fiber communication systems. We have also discussed various PMD statistics of such a model, and we have demonstrated that the outage statistics of isotropic and anisotropic hinge models behave very differently from one another. In particular, the waveplate hinge model predicts smaller values of NCR in the range of outage probabilities of interest. These results clearly indicate that PMD-induced outages depend on the specific details of the manner in which PMD is physically generated in the system. Thus, the issue of what is the correct physical model to describe PMD in actual installed systems appears to deserve further study.

We thank P. J. Winzer for many insightful discussions. This work was supported by the National Science Foundation under grants DMS-0506101 and DMS-0709070.

References

1. M. Brodsky, M. Boroditsky, P. Magill, N. J. Frigo, and M. Tur, Opt. Express **13**, 4090 (2005).
2. M. Boroditsky, M. Brodsky, P. Magill, N. J. Frigo, C. Antonelli, and A. Mecozzi, IEEE Photon. Technol. Lett. **17**, 345 (2005).
3. C. Antonelli and A. Mecozzi, J. Lightwave Technol. **24**, 4064 (2006).
4. M. Brodsky, N. J. Frigo, M. Boroditsky, and M. Tur, J. Lightwave Technol. **24**, 4584 (2006).
5. M. Brodsky, J. C. Martinez, N. J. Frigo, and A. Sirenko, in *Proceedings of the European Conference on Optical Communication (ECOC)* (IEEE, 2005), Vol. 3, p. 335.
6. W. Shieh and H. Kogelnik, IEEE Photon. Technol. Lett. **13**, 40 (2001).
7. J. P. Gordon and H. Kogelnik, Proc. Natl. Acad. Sci. USA **97**, 4541 (2000).
8. G. Biondini, W. L. Kath, and C. R. Menyuk, IEEE Photon. Technol. Lett. **14**, 310 (2002).
9. S. L. Fogal, G. Biondini, and W. L. Kath, IEEE Photon. Technol. Lett. **14**, 1273 (2002).
10. G. Biondini, W. L. Kath, and C. R. Menyuk, J. Lightwave Technol. **22**, 1201 (2004).
11. P. T. De Boer, D. P. Kroese, S. Mannor, and R. Y. Rubinstein, Ann. Operat. Res. **134**, 19 (2005).
12. R. Barakat, J. Phys. A **6**, 796 (1973).
13. H. Kogelnik, P. J. Winzer, L. E. Nelson, R. M. Jopson, M. Boroditsky, and M. Brodsky, IEEE Photon. Technol. Lett. **17**, 1208 (2005).